

Constraint Based Refinement of Optical Flow

Hirak Doshi, N. Uday Kiran

Department of Mathematics and Computer Science
Sri Sathya Sai Institute of Higher Learning
{hirakdoshi, nudaykiran}@sssihl.edu.in

Abstract

The goal of this paper is to formulate a general framework for a constraint-based refinement of the optical flow using variational methods. We demonstrate that for a particular choice of the constraint, formulated as a minimization problem with the quadratic regularization, our results are close to the continuity equation based fluid flow. This closeness to the continuity model is theoretically justified through a modified augmented Lagrangian method and validated numerically. Further, along with the continuity constraint, our model can include geometric constraints as well. The correctness of our process is studied in the Hilbert space setting. Moreover, a special feature of our system is the possibility of a diagonalization by the Cauchy-Riemann operator and transforming it to a diffusion process on the curl and the divergence of the flow. Using the theory of semigroups on the decoupled system, we show that our process preserves the spatial characteristics of the divergence and the vorticities. We perform several numerical experiments and show the results on different datasets.

Keywords. Optical Flow, Fluid Flow, Variational Formulation, Diffusion Process, Augmented Lagrangian, Multiplicative Perturbation of the Laplacian.

Mathematics Subject Classification 2020. 35J50, 35Q68.

1 Introduction

Variational models for motion estimation have always been one of the central topics in Mathematical Image Processing. Since the seminal work on the variational approach to optical flow motion estimation of Horn and Schunck [17], many in-depth studies on this topic have been done through developing different variational models of optical flow to obtain useful insights into motion estimation (e.g. [22, 3, 16, 25]). Many of these literature works on motion estimation has been focused on the constancy assumption e.g., the brightness constancy leading to an algebraic equation, in (u, v) the motion components, called the optical flow constraint (OFC) :

$$f_\tau + f_x u + f_y v = 0, \quad (1)$$

where $f(x, y, \tau)$ is the image sequence $f : \Omega \times [0, \infty) \rightarrow \mathbb{R}$ for an open bounded set $\Omega \subset \mathbb{R}^2$, (x, y) are the spatial coordinates and τ is the time variable. However, constancy assumptions can't reflect the reality of actual motion because deformation effects

of fluid, illumination variations, perspective changes, poor contrast etc. would directly affect the important motion parameters being physics-dependent. For this reason, physics-dependent motion estimation algorithms have been widely investigated.

A relatively recent and representative work of Corpetti et.al. [7], in which fluid mechanics was used to extending the optical flow estimation, and accurate dense motion fields were obtained. This method includes an image-based integrated version of the continuity equation from fluid dynamics. Since then more attention has been gained on studying the physics-based motion estimation. Estimates on the conservation of mass for a fluids in a digital image sequence was discussed by Wildes et.al. [26]. They model the image intensity as an average of the object density and consider the incident light parallel to the z -axis the 2D projection of the image intensity

$$f(x, y, \tau) = \int_{z_1}^{z_2} \rho(x, y, z, \tau) dz.$$

Further using fluid mechanics models Liu et.al. [24] provided a rigorous framework for an optical approach to fluid flow by deriving the projected-motion equations where the optical flow is proportional to the path-averaged velocity of fluid or particles weighted with a relevant field quantity. In this approach the authors assume that the control surface is planar, there is no particle diffusion by a molecular process, and the rate of accumulation of the particle in laser sheet illuminated volume is neglected, the equations, after neglecting these terms one obtains the continuity equation again. Assuming that the flow field governing the advection is the gradient of a potential function (resp. symplectic gradient of a stream function) Luttmann et.al. [20] computed the potential (resp. stream) function directly. To preserve the spatial characteristics of divergence and vorticities in the flow the authors in [8] proposed a regularizing functional based on divergence and curl. They discussed the shortcomings of the first-order regularization in flow measurements and suggested a regularization functional based on the gradients of divergence and curl to preserve the spatial characteristics of divergence and vorticity in flows. Use of this second-order div-curl (divergence and curl) regularization is more plausible conceptually to preserve fine structures in turbulent flows. A detailed account of various works in the fluid flow based on physics is given in [14]. Here the authors observed a physical meaning associated with the terms of the continuity equation (CEC) :

$$\underbrace{f_\tau + f_x u + f_y v}_{\text{(a)}} + \underbrace{f(u_x + v_y)}_{\text{(b)}} = 0; \quad (2)$$

(a) corresponds to the brightness constancy given in (1) and **(b)** accounts for the non-conservation of the brightness function due to loss of particles caused by non-null out of plane component. Furthermore, a divergence-free approximation of the equation (2) could be obtained by setting the term **(b)** to zero. It is thus natural to study the effect of the term **(b)** in extracting the inherent fluid properties of the flow.

In this paper our motivation is to understand and build a generic physics constraint-based framework for the fluid flow estimation. Taking a cue from the observation in [14] on the Equation (2), we propose a model to capture the additional constraint induced by an underlying non-conservation phenomenon. Given an initial field (u_0, v_0) obtained by the brightness constancy based optical flow, we consider the following image driven

evolutionary PDE model to modify the flow:

$$\begin{cases} \frac{\partial u}{\partial t} = \Delta u + a_0 \frac{\partial}{\partial x} [\phi(f)(u_x + v_y)] \\ \frac{\partial v}{\partial t} = \Delta v + a_0 \frac{\partial}{\partial y} [\phi(f)(u_x + v_y)], \end{cases} \quad (3)$$

where a_0 is a positive constant and the function ϕ is dependent on the application at hand. We show that the system (3) is well-posed in the Hilbert space $H^1(\Omega) \times H^1(\Omega)$. We further demonstrate that for a particular choice of the additional constraint our model closely approximates the continuity model. We use a modified augmented Lagrangian framework to show this equivalence.

A special feature of our model (3) is the diagonalization by the Cauchy-Riemann operator to obtain an implicit diffusion process

$$\frac{\partial \xi}{\partial t} = \Delta \xi \quad \text{and} \quad \frac{\partial \zeta}{\partial t} = \Delta (k\zeta), \quad (4)$$

where $\xi := u_y - v_x$ is the curl and $\zeta := u_x + v_y$ is the divergence of the flow and $k = 1 + a_0\phi(f)$ is a multiplicative factor. Here the diffusion process is image dependent as a multiplicative perturbation of the Laplacian on the divergence; thereby leading to a reinterpretation of the continuity model as a transport phenomenon induced as “diffusive fluxes” expressed as functions of gradient quantities. In physics, a similar diffusion phenomenon is observed for the gradient quantities for the fluid flow of ideal gases and plasmas in [23]. Moreover, in the paper [19] the authors observe a path-averaging behaviour of the velocities which further justifies the underlying a diffusive behaviour.

The incompressibility condition implies that the density remains constant within a parcel of fluid that moves with the flow velocity. Even compressible flows can be locally modelled as an incompressible flow. The OFC can be viewed as a divergence-free approximation of the CEC based model (although this view is not exact, in our algorithm we start with this approximation), see [19, 6]. This is the starting point of our discussion. Having obtained a crude approximation from the Horn and Schunck optical flow in the next phase we obtain a refinement by choosing specific additional constraints. The main advantage of our method is firstly from a theoretical point of view it provides us with an evolutionary PDE setup which allows a rigorous mathematical framework for the well-posedness discussion. Secondly, due to the semigroup approach, we can have a simpler analysis and also obtain faster convergence of the solution in our scheme.

As described in the subsequent section we will formulate the variational problem, with the quadratic regularizer, as an approximation to the one associated with the CEC model (again with a quadratic regularizer). We adopt a modified augmented Lagrangian framework to justify the reason for closeness. A modified Bounded Constraint Algorithm is employed, where the modification corresponds to the Lagrangian multiplier also accounting for the divergence term. The inner iterations of the algorithm use the contractive semigroup of the elliptic term. We also demonstrate the results numerically.

This approach thus allows us to build a quantitative connection between the optical flow and the fluid flow for various flow visualizations which is often a key problem. Further, our method has a direct implication to the variational formulation in the deep learning paradigm. In the current work, we focus on the flow visualization problem although our approach could be adopted to other variational problems as well.

The paper is organized as follows: Section 2 deals with the mathematical framework of our study. This discussion is divided into multiple subsections. In Subsection 2.1 we

describe of our constraint-based refinement formulation. We then discuss the existence, uniqueness of our model. Subsequently, in Subsection 2.2 we discuss the decoupling and diagonalization of our system by the Cauchy-Riemann operator. We then study the decoupled system in Sobolev spaces discussing the multiplicative perturbation of the laplacian of the divergence of the flow in Subsection 2.2.1. In Subsection 2.3 for a specific choice of additional constraint, we show the equivalence of our model to the CEC based model using the Augmented Lagrangian framework. We give a description of the bounded constraint algorithm and the implementation details of the system in Subsection 2.3.1. Finally, we show the results obtained by our algorithm on different datasets in Section 3.

2 Mathematical Framework

2.1 Description of the Model

Our main objective is to obtain a refinement of a flow field preserving certain intrinsic spatial characteristics. As a concrete example, we choose to refine the Horn and Schunck optical flow [17]. The main advantage of this formulation is the mathematical well-posedness [22]. Even though it is well-known that this model is not adequate for problems corresponding to fluid flow visualization [8, 7, 18] nevertheless, it is a reasonable starting point for pixel correspondence even for fluid flow [18]. With this background, we propose the following formulation

$$J_R(\mathbf{u}) = \beta \int_{\Omega} \phi(f) \psi(\nabla \mathbf{u}) + \alpha \int_{\Omega} \{|\nabla u|^2 + |\nabla v|^2\}, \quad (5)$$

subjected to the bounded optical flow constraint

$$\|f_{\tau} + \nabla f \cdot \mathbf{u}\|_{L^2}^2 \leq \epsilon,$$

where ψ depends on the components of the flow and it's derivatives and ϕ corresponds to an image-dependent weight term which makes the refinement process image-driven. If $\phi(f) \equiv 1$ then the refinement process is completely flow-driven. The constants α, β are weight parameters. We assume that both the functions ϕ and ψ are real-valued smooth functions. Moreover, we assume ϕ a monotone increasing function. The first term of $J_R(\mathbf{u})$ captures the non-conservation term that violate the constancy assumptions and the second term is the L^2 regularization which governs the diffusion phenomena. The bounded constraint formulated along the lines of the Horn and Schunck governs the apriori ‘divergence-free’ estimate for the pixel correspondence. The rational for the choice of the constraint will be discussed later. The tolerance threshold ϵ is dictated by the error estimates of the Horn and Schunck given in [18]. In the current work we particularly focus on the case where $\psi = (\nabla \cdot \mathbf{u})^2$, i.e. where ψ penalizes the divergence of the flow. In this case the refinement functional becomes

$$J_R(\mathbf{u}) = \beta \int_{\Omega} \phi(f) (\nabla \cdot \mathbf{u})^2 + \alpha \int_{\Omega} \{|\nabla u|^2 + |\nabla v|^2\}. \quad (6)$$

The Euler-Lagrange equations lead to a second-order, linear, coupled elliptic system. The ellipticity is clear as the integrand

$$F(x, \mathbf{u}, \nabla \mathbf{u}) := \beta \phi(f) (\nabla \cdot \mathbf{u})^2 + \alpha (|\nabla u|^2 + |\nabla v|^2),$$

satisfies the Legendre-Hadamard condition

$$\begin{aligned} \sum_{i,j=1}^2 \sum_{\alpha,\beta=1}^2 \frac{+\partial^2 F}{\partial \theta_{i\alpha} \partial \theta_{j\beta}}(\theta) \gamma_i \gamma_j \mu_\alpha \mu_\beta &= 2\alpha_2(\gamma_1^2 + \gamma_2^2)(\mu_1^2 + \mu_2^2) + 2\beta\phi(f)(\gamma_1\mu_1 + \gamma_2\mu_2)^2 \\ &= 2\alpha_2|\gamma|^2 |\mu|^2 + 2\beta\phi(f)(\gamma \cdot \mu)^2 \geq 0, \end{aligned}$$

where we have denoted $\nabla \mathbf{u}$ by θ and the components by $\theta_{ij}, i = 1, 2$ and $j = 1, 2$. We also require the functional to be convex and coercive so that the mathematical well-posedness is guaranteed (see for instance Section 8.2.4, Theorems 5 and 6 in [12]). The convexity part is easy to show. The coercivity can be seen as follows. Let us write the integrand F as

$$F(\theta) = \alpha_2|\theta|^2 + \beta\phi(f)(\text{tr } \theta)^2,$$

where $\text{tr } \theta$ denotes the trace of the matrix θ . Let us call $h(\theta) := \phi(f)(\text{tr } \theta)^2$. Now since h is convex wrt θ , we have

$$h(\theta) \geq h(0) + \nabla h(0) \cdot \theta \quad \forall \theta.$$

Therefore,

$$\begin{aligned} F(\theta) &\geq \alpha_2|\theta|^2 + \beta(h(0) + \nabla h(0) \cdot \theta) \\ &\geq \alpha_2|\theta|^2 + \beta\left(h(0) - \frac{1}{2}2|\nabla h(0)||\theta|\right) \\ &\geq \alpha_2|\theta|^2 + \beta h(0) - \frac{1}{2}\beta(|\nabla h(0)|^2 + |\theta|^2) \\ &\geq \left(\alpha_2 - \frac{1}{2}\beta\right)|\theta|^2 + \beta h(0) - \frac{1}{2}\beta|\nabla h(0)|^2 \\ &= a_1|\theta|^2 + a_2, \end{aligned}$$

where $a_1 = \alpha_2 - \frac{1}{2}\beta$ and $a_2 = \beta h(0) - \frac{1}{2}\beta|\nabla h(0)|^2$. Thus we have shown the well-posedness of our model. We are now interested in the mathematical analysis of our system. Several sophisticated mathematical tools exist can be employed to this end [5, 9, 4, 21]. We will study the following parabolic system

$$\left\{ \begin{array}{l} \frac{\partial u}{\partial t} = \Delta u + a_0 \frac{\partial}{\partial x}[\phi(f)(u_x + v_y)] \text{ in } \Omega \times (0, \infty), \\ \frac{\partial v}{\partial t} = \Delta v + a_0 \frac{\partial}{\partial y}[\phi(f)(u_x + v_y)] \text{ in } \Omega \times (0, \infty), \\ u(x, y, 0) = u_0 \text{ in } \Omega, \\ v(x, y, 0) = v_0 \text{ in } \Omega, \\ \frac{\partial u}{\partial n} = 0 \text{ on } \partial\Omega \times (0, \infty), \\ \frac{\partial v}{\partial n} = 0 \text{ on } \partial\Omega \times (0, \infty), \end{array} \right. \quad (7)$$

using an evolutionary PDE approach. Here (u_0, v_0) is the feasible solution obtained through the bounded constraint by the Horn and Schunck optical flow. The Neumann boundary condition is a natural choice in image processing as it ensures no additional details or edges are created at the boundary.

2.2 Diagonalization of the System

In this section we will show that the system (3) can be diagonalized by an application of Cauchy-Riemann operator. This special feature is intriguing as well as of great advantage for later analysis. Let us first rewrite the system (3) as

$$\frac{\partial \mathbf{u}}{\partial t} = A\mathbf{u}, \quad (8)$$

where

$$\frac{\partial \mathbf{u}}{\partial t} = \begin{bmatrix} \frac{\partial u}{\partial t} \\ \frac{\partial v}{\partial t} \end{bmatrix}, \quad A\mathbf{u} = \begin{bmatrix} \Delta u + a_0 \frac{\partial}{\partial x} [\phi(f)(u_x + v_y)] \\ \Delta v + a_0 \frac{\partial}{\partial y} [\phi(f)(u_x + v_y)] \end{bmatrix}.$$

As we are in the Sobolev setting, the derivatives are taken in a distributional sense. Thus, a key observation is that the order of derivatives can be interchanged. Let us denote by R the Cauchy-Riemann operator matrix

$$R = \begin{bmatrix} \partial_y & -\partial_x \\ \partial_x & \partial_y \end{bmatrix}.$$

Acting R on both sides of (8) leads to

$$R\left(\frac{\partial \mathbf{u}}{\partial t}\right) = RA\mathbf{u}.$$

This leads to the following transformation of the original coupled system

$$\begin{aligned} \begin{bmatrix} \partial_y & -\partial_x \\ \partial_x & \partial_y \end{bmatrix} \begin{bmatrix} \frac{\partial u}{\partial t} \\ \frac{\partial v}{\partial t} \end{bmatrix} &= \begin{bmatrix} \partial_y & -\partial_x \\ \partial_x & \partial_y \end{bmatrix} \begin{bmatrix} \Delta u + a_0 \frac{\partial}{\partial x} [\phi(f)(u_x + v_y)] \\ \Delta v + a_0 \frac{\partial}{\partial y} [\phi(f)(u_x + v_y)] \end{bmatrix} \\ &= \begin{bmatrix} \Delta & 0 \\ 0 & \Delta \circ k \end{bmatrix} \begin{bmatrix} \partial_y & -\partial_x \\ \partial_x & \partial_y \end{bmatrix} \begin{bmatrix} u \\ v \end{bmatrix}, \end{aligned}$$

where with a slight abuse of notation we denote k for the function $1 + a_0\phi(f)$ and for the multiplicative operator $x \mapsto kx$. Since ϕ is a bounded function and $a_0 > 0$, the multiplicative term k is bounded and strictly positive. We have thus obtained the following decoupling:

$$\frac{\partial}{\partial t}(R\mathbf{u}) = DR\mathbf{u}, \quad (9)$$

where

$$D = \begin{bmatrix} \Delta & 0 \\ 0 & \Delta \circ k \end{bmatrix}, \quad R = \begin{bmatrix} \partial_y & -\partial_x \\ \partial_x & \partial_y \end{bmatrix}.$$

The application of the Cauchy-Riemann operator R on the system has resulted in the following relation

$$D = RAR^{-1}.$$

The operator A has been diagonalized by the matrix R . The decoupled system (9) thus takes the following form:

$$\begin{cases} \frac{\partial \xi}{\partial t} = \Delta \xi, \\ \frac{\partial \zeta}{\partial t} = \Delta(k\zeta), \end{cases} \quad (10)$$

where $\xi := u_y - v_x$ is the curl and $\zeta := u_x + v_y$ is the divergence of the flow and $k = 1 + a_0\phi(f)$ is a multiplicative factor.

Remark 1. Observe that if $\alpha = 0$, i.e. in the absence of the regularization term, the system (10) reduces to

$$\begin{cases} \frac{\partial \xi}{\partial t} = 0, \\ \frac{\partial \zeta}{\partial t} = \beta \Delta(\phi(f)\zeta). \end{cases} \quad (11)$$

The first equation means the vorticities will remain unchanged. On the other hand, for the divergence equation, we have a degeneracy at the null values of the image function f . Thus, as expected by the aperture problem, this leads to an ill-posed problem.

Let us consider the abstract IVP associated with the first equation in (10):

$$\begin{cases} \frac{d\xi}{dt} + A_1\xi = 0 \text{ on } [0, \infty), \\ \xi(0) = \xi_0 \in L^2(\Omega). \end{cases} \quad (12)$$

where the initial data

$$\xi_0 = \partial_y u_0 - \partial_x v_0,$$

and (u_0, v_0) is the Horn and Schunck optical flow. Here $A_1 : D(A_1) \rightarrow H_1$ is an (unbounded) operator

$$\begin{cases} D(A_1) = \{\xi \in H^2(\Omega) \cap H_0^1(\Omega) : A_1\xi \in L^2(\Omega)\}, \\ H_1 = L^2(\Omega), \\ A_1\xi := -\Delta\xi. \end{cases}$$

The operator A_1 is maximal monotone and symmetric. Hence it is self adjoint. For the well-posedness of the problem (12) we refer to (Theorem 7.7 and 10.1 in [5]). We will prove similar results for the second equation.

2.2.1 Multiplicative Perturbation of the Laplacian

Let us consider the divergence equation from (10)

$$\frac{\partial \zeta}{\partial t} = \Delta(k\zeta), \quad (13)$$

where $k = 1 + a_0\phi(f)$. We make a change of variable $\eta = k\zeta$. The abstract IVP thus becomes

$$\begin{cases} \frac{d\eta}{dt} + A_2\eta = 0 \text{ on } [0, \infty), \\ \eta(0) = \eta_0 \in L^2(\Omega). \end{cases} \quad (14)$$

where the initial data

$$\eta_0 = k(\partial_x u_0 + \partial_y v_0),$$

is the weighted divergence of the Horn and Schunck optical flow. Here $A_2 : D(A_2) \rightarrow H_2$ is the (unbounded) operator

$$\begin{cases} D(A_2) = \{\eta \in H^2(\Omega) \cap (H_0^1)_k(\Omega) : A_2\eta \in L_k^2(\Omega)\}, \\ H_2 = L_k^2(\Omega), \\ A_2\eta = -k\Delta\eta. \end{cases}$$

Also $\eta_0 \in L^2(\Omega)$. Here the operator $k\Delta$ is a multiplicative perturbation of the laplacian where k is bounded and strictly positive since ϕ is a monotone increasing function. The problem will be studied in weighted Sobolev space $L_k^2(\Omega)$ following a similar approach as in [11]. The space $L_k^2(\Omega)$ is a Hilbert space equipped with the inner product

$$\langle w_1, w_2 \rangle_{L_k^2} := \int_{\Omega} \frac{1}{k} w_1 w_2 \, dx$$

and the norm

$$\|w\|_{L_k^2}^2 = \int_{\Omega} \frac{1}{k} |w|^2 \, dx.$$

Similarly the Hilbert space $(H_0^1)_k(\Omega)$ has the norm [11]

$$\|w\|_{(H_0^1)_k}^2 := \|w\|_{L_k^2}^2 + \|\nabla w\|_{L^2}^2 = \int_{\Omega} \left(\frac{1}{k} |w|^2 + |\nabla w|^2 \right).$$

It is interesting to note that in our context the weight term k in $L_k^2(\Omega)$ is actually dependent on the image f - bringing in an anisotropy into the discussion. Thus $L_k^2(\Omega)$ is an image dependent Sobolev space. When $\phi(f)$ is a constant function, i.e. the case where the refinement is independent of the image, the norms $\|\cdot\|_2$ and $\|\cdot\|_{L_k^2}$ coincide upto a constant. In our context, as the values of the image are bounded, k is a bounded function. Also in the pre-processing stage since the images are smoothened with a Gaussian filter we can further assume that k is smooth. It is easy to show the topological equivalence of the spaces $L^2(\Omega)$ and $L_k^2(\Omega)$. We now prove a result on the regularity of the solution for any non-zero time in the diffusion process. We need several lemmas before proving the main result.

Lemma 1. The operator A_2 is symmetric in $L_k^2(\Omega)$.

Proof.

$$\begin{aligned}\langle A_2 w_1, w_2 \rangle &= \int_{\Omega} \frac{1}{k} (-k \Delta w_1) w_2 = \int_{\Omega} \nabla w_1 \nabla w_2 \\ \langle w_1, A_2 w_2 \rangle &= \int_{\Omega} \frac{1}{k} w_1 (-k \Delta w_2) = \int_{\Omega} \nabla w_1 \nabla w_2.\end{aligned}\quad \square$$

Lemma 2. The operator A_2 is maximal monotone in $L_k^2(\Omega)$.

Proof. Observe that

$$\langle A_2 w, w \rangle = \int_{\Omega} \frac{1}{k} (-k \Delta w) w = \int_{\Omega} |\nabla w|^2 \geq 0.$$

This shows that the operator A_2 is monotone. To show maximal monotonicity we need to show that $R(I + A_2) = H_2$, i.e. for a given $g \in L_k^2(\Omega)$ we have to find a unique $w \in D(A_2)$ such that

$$w - k \Delta w = g,$$

holds. Dividing both sides by k we obtain

$$\frac{1}{k} w - \Delta w = \frac{g}{k}. \quad (15)$$

The equivalent weak form of Equation (15) reads

$$a(w, w') := \int_{\Omega} \left(\frac{1}{k} w w' + \nabla w \nabla w' \right) = \int_{\Omega} \frac{1}{k} g w' =: b(w'), \quad (16)$$

for all $w' \in (H_0^1)_k(\Omega)$. Since Ω is bounded, by using the topological equivalence of $L^2(\Omega)$ and $L_k^2(\Omega)$ and (Proposition 4.5 in [15]) we conclude that there is a unique $w \in D(A_2)$ such that $w - k \Delta w = g$ holds. Moreover, $w \in H^2(\Omega)$ and

$$\|w\|_{H^2} \leq C \|g\|_{L_k^2} \leq 2C^2 (\|w\|_{L_k^2} + \|\nabla w\|_{L^2}). \quad \square$$

Now, we prove a regularity theorem for the initial value problem (14). The result also provides us with a infinite propagation behavior of the solution.

Theorem 1. Let $\eta_0 \in L^2(\Omega)$. Then the solution of the problem (14) satisfies

$$\eta \in C^1((0, \infty), L_k^2(\Omega)) \cap C([0, \infty), H^2(\Omega) \cap (H_0^1)_k(\Omega)).$$

For any $\epsilon > 0$ we also have

$$\eta \in C^\infty([\epsilon, \infty) \times \bar{\Omega}). \quad (17)$$

Moreover, $\eta \in L^2((0, \infty), (H_0^1)_k(\Omega))$, and

$$\frac{1}{2} \|\eta(T)\|_{L^2}^2 + \int_0^T \|\nabla \eta(t)\|_{L^2}^2 dt = \frac{1}{2} \|\eta_0\|_{L_k^2}^2 \quad (18)$$

holds for $T > 0$.

Proof. By Lemma 1 and 2 the operator A_2 is symmetric and maximal monotone. Hence it is self-adjoint. Therefore, by Theorem 7.7 in [5], we have

$$\eta \in C^1((0, \infty), L_k^2(\Omega)) \cap C([0, \infty), H^2(\Omega) \cap (H_0^1)_k(\Omega)).$$

Define $\sigma(t) = \frac{1}{2}\|\eta(t)\|_{L_k^2}^2$. Since $\eta \in C^1((0, \infty), L_k^2(\Omega))$ it is clear that σ is C^1 on $(0, \infty)$. Therefore

$$\begin{aligned}\sigma'(t) &= \left\langle \eta(t), \frac{d\eta}{dt}(t) \right\rangle_{L_k^2} \\ &= \left\langle \eta(t), k\Delta\eta \right\rangle_{L_k^2} \\ &= \left\langle \eta(t), \Delta\eta \right\rangle_{L^2} \\ &= -\|\nabla\eta(t)\|_{L^2}^2.\end{aligned}$$

Integrating from ε to T where $0 < \varepsilon < T < \infty$ we get

$$\sigma(T) - \sigma(\varepsilon) = - \int_{\varepsilon}^T \|\nabla\eta(t)\|_{L^2}^2 dt.$$

Again as $\eta \in C((0, \infty), L_k^2(\Omega))$ we have $\sigma(\varepsilon) \rightarrow \sigma(0) = \frac{1}{2}\|\eta_0\|_{L_k^2}^2$ as $\varepsilon \rightarrow 0$. Therefore in the limiting case we obtain

$$\sigma(T) + \int_0^T \|\nabla\eta(t)\|_{L^2}^2 dt = \frac{1}{2}\|\eta_0\|_{L_k^2}^2,$$

and (18) holds. Integrating the Hilbert space $(H_0^1)_k(\Omega)$ norm defined above from 0 to T we get

$$\begin{aligned}\int_0^T \|\eta(t)\|_{(H_0^1)_k}^2 dt &= \int_0^T \|\eta(t)\|_{L_k^2}^2 dt + \int_0^T \|\nabla\eta(t)\|_{L^2}^2 dt \\ &= 2 \int_0^T \sigma(t) dt + \int_0^T \|\nabla\eta(t)\|_{L^2}^2 dt \\ &\leq 2 \int_0^T \sigma(t) dt + \frac{1}{2}\|\eta_0\|_{L_k^2}^2.\end{aligned}$$

This shows that

$$\eta \in L^2((0, \infty), (H_0^1)_k(\Omega)).$$

Finally, to show (17) consider $D(A_2) = \{u \in H^2(\Omega) \cap (H_0^1)_k(\Omega) : A_2 u \in L_k^2(\Omega)\}$. Note that $D(A_2) \subset (H_0^1)_k(\Omega)$. Thus $\eta \in D(A_2)$ implies $\eta = 0$ on $\partial\Omega$. We first show that

$$D(A_2^l) = \{\eta \in H^{2l}(\Omega) : \eta = \Delta\eta = \dots = \Delta^{l-1}\eta = 0 \text{ on } \partial\Omega\} \quad \forall l \geq 1. \quad (19)$$

To show this we will use induction on l . The case $l = 1$ is clear from the above discussion where

$$D(A_2) = H^2(\Omega) \cap (H_0^1)_k(\Omega) = \{\eta \in H^2(\Omega) : \eta = 0 \text{ on } \partial\Omega\}.$$

Let us assume that (19) holds for $l - 1$, i.e.

$$D(A_2^{l-1}) = \{\eta \in H^{2l-2}(\Omega) : \eta = \Delta\eta = \dots = \Delta^{l-2}\eta = 0 \text{ on } \partial\Omega\}. \quad (20)$$

Observe that

$$D(A_2^l) = \{\eta \in D(A_2^{l-1}) : A_2\eta \in D(A_2^{l-1})\}.$$

Now $\eta \in D(A_2^{l-1})$ implies $\eta \in H^{2l-2}(\Omega)$ and $\eta = \Delta\eta = \dots = \Delta^{l-2}\eta = 0$ on $\partial\Omega$. Also $A_2\eta \in D(A_2^{l-1})$ implies $k\Delta\eta \in H^{2l-2}(\Omega)$ and $\Delta\eta = \dots = \Delta^{l-1}\eta = 0$ on $\partial\Omega$. Thus we have

$$\eta \in H^{2l-2}(\Omega) \text{ and } k\Delta\eta \in H^{2l-2}(\Omega),$$

and thus there is a unique $g \in H^{2l-2}(\Omega)$ such that $\eta - k\Delta\eta = g$ holds. Moreover $\eta \in H^{2l}(\Omega)$. This shows that

$$D(A_2^l) \subset \{\eta \in H^{2l}(\Omega) : \eta = \Delta\eta = \dots = \Delta^{l-1}\eta = 0 \text{ on } \partial\Omega\}. \quad (21)$$

On the other hand if $\eta \in H^{2l}(\Omega)$ and $\eta = \Delta\eta = \dots = \Delta^{l-1}\eta = 0$ on $\partial\Omega$ then $A_2\eta = -k\Delta\eta \in H^{2l-2}(\Omega)$ and $A_2\eta = \dots = \Delta^{l-1}(A_2\eta) = 0$ on $\partial\Omega$. Then by induction hypothesis $\eta \in D(A_2^{l-1})$ and $A_2\eta \in D(A_2^{l-1})$ so that

$$\{\eta \in H^{2l}(\Omega) : \eta = \Delta\eta = \dots = \Delta^{l-1}\eta = 0 \text{ on } \partial\Omega\} \subset D(A_2^l).$$

Combining this and (21) we obtain (19). Next we show that $D(A_2^l) \subset H^{2l}$ is a continuous injection for all $l \geq 1$. To show that we will show that $\|\eta\|_{H^{2l}} \rightarrow 0$ as $\|\eta\|_{D(A_2^l)} \rightarrow 0$. We again use induction to show this fact. For the base case $l = 1$ observe that if $\eta \in H^2(\Omega) \cap (H_0^1)_k(\Omega)$ then there exists a unique $g \in L_k^2(\Omega)$ such that

$$\eta - k\Delta\eta = g,$$

and

$$\|\eta\|_{H^2} \leq C\|g\|_{L_k^2} \leq 2C^2(\|\eta\|_{L_k^2} + \|\Delta\eta\|_{L^2}).$$

Clearly, $\|\eta\|_{D(A_2)} \rightarrow 0$ implies $\|\eta\|_{L_k^2}, \|\Delta\eta\|_{L^2} \rightarrow 0$ and thus $\|\eta\|_{H^2} \rightarrow 0$. Let us assume that the same holds for $l - 1$, i.e. $D(A_2^{l-1}) \subset H^{2l-2}$ be a continuous injection. Let $\eta \in D(A_2^l)$. Then $-k\Delta\eta \in H^{2l-2}$ and using similar argument as above we see that

$$\|\eta\|_{H^{2l}} \leq 2C^2(\|\eta\|_{H^{2l-2}} + \|\Delta\eta\|_{H^{2l-2}}).$$

Thus $\|\eta\|_{D(A_2^l)}^2 = \sum_{i=0}^l \|A_2^i\eta\|_{L_k^2}^2 = \|A_2\eta\|_{L_k^2}^2 + \|\eta\|_{D(A_2^{l-1})}^2$.

Therefore $\|\eta\|_{D(A_2^l)}^2 \rightarrow 0 \implies \|\eta\|_{D(A_2^{l-1})}^2 \rightarrow 0$. This shows that $\|\eta\|_{H^{2l-2}}, \|\Delta\eta\|_{H^{2l-2}} \rightarrow 0$ and hence $\|\eta\|_{H^{2l}} \rightarrow 0$. This completes the induction. Thus

$$\eta \in C^m((0, \infty), H^{2l}(\Omega)) \forall m \in \mathbb{N}.$$

By one of the corollaries of Sobolev embedding theorem there is an $l > m$ such that the injection $H^l(\Omega) \subset C^m(\overline{\Omega})$ is continuous. Therefore the injection $H^{2l}(\Omega) \subset H^l(\Omega) \subset C^m(\overline{\Omega})$ is continuous and consequently

$$\eta \in C^m((0, \infty), C^m(\overline{\Omega})) \forall m \in \mathbb{N}.$$

Hence we can conclude that

$$\eta \in C^\infty([\varepsilon, \infty) \times \overline{\Omega}) \forall \varepsilon > 0.$$

This completes the proof. \square

Multiplicative perturbation of the laplacian arises in many physical phenomena e.g. in the theory of wave propagation in non-homogeneous media. The operator has been studied in appropriate weighted function spaces see [11, 2]. In our case the multiplicative perturbation $k\Delta$ leads to an image driven perturbation because of the k factor which depends on the image f . The authors in [2] derive an approximation for the kernel of the associated semigroups by positive linear integral operators

$$G_m(f)(x) = \left(\frac{m}{4\pi k(x)}\right)^{n/2} \int_{\mathbb{R}^n} f(y) \exp\left(-\frac{m}{4k(x)}\|x-y\|^2\right) dy. \quad (22)$$

Using the above kernel one can design an appropriate stencil for convolution. It is also interesting to note that the stencil size varies with respect to the image intensity. This aspect we will discuss in a forthcoming paper. Let us now consider the Gaussian kernel associated with the operator $k\Delta$

$$G_k(x, t) := \frac{1}{4\pi k(x)t} \exp\left(-\frac{|x|^2}{4k(x)t}\right).$$

The perturbation k plays an important role in controlling the rate of diffusion. If k is large then the Gaussian becomes broader and shorter and if it is small then the Gaussian is thinner and taller. Using the boundedness of k , i.e. $a_1 \leq k(x) \leq a_2$ we can obtain an estimate of the p -norm of $G_k(x, t)$ as the following lemma shows.

Lemma 3. Let $n = 2$. Then

$$\|G_k(x, t)\|_p \leq C_k t^{(1-p)/p},$$

where the constant

$$C_k = \frac{1}{4\pi a_1} \left(\frac{4\pi a_2}{p}\right)^{1/p}.$$

Proof.

$$\begin{aligned} \|G_k(x, t)\|_p^p &= \int_{\mathbb{R}^2} \left(\frac{1}{4\pi k(x)t}\right)^p \exp\left(-\frac{p|x|^2}{4k(x)t}\right) dx \\ &\leq \left(\frac{1}{4\pi a_1 t}\right)^p \int_{\mathbb{R}^2} \exp\left(-\frac{p|x|^2}{4k(x)t}\right) dx \\ &\leq \left(\frac{1}{4\pi a_1 t}\right)^p \int_{\mathbb{R}^2} \exp\left(-\frac{p|x|^2}{4a_2 t}\right) dx \end{aligned}$$

Make a change of variable $x = (ta_2/p)^{1/2}y$. Thus we obtain

$$\begin{aligned} \|G_k(x, t)\|_p^p &\leq \left(\frac{1}{4\pi a_1 t}\right)^p \left(\frac{ta_2}{p}\right) \int_{\mathbb{R}^2} \exp\left(-\frac{|y|^2}{4}\right) dy \\ &= 4\pi \left(\frac{1}{4\pi a_1}\right)^p \left(\frac{a_2}{p}\right) t^{1-p}. \end{aligned}$$

Thus

$$\|G_k(x, t)\|_p \leq \frac{1}{4\pi a_1} \left(\frac{4\pi a_2}{p}\right)^{1/p} t^{(1-p)/p} \leq C_k t^{(1-p)/p}.$$

□

To conclude the discussion on the transformation we have to also ensure that nothing bad happens due to the inverse transformation

$$R^{-1} = \Delta^{-1} \begin{bmatrix} \partial_y & \partial_x \\ -\partial_x & \partial_y \end{bmatrix},$$

where Δ^{-1} is the inverse of the Laplacian. Indeed, this is the case by the virtue of the ellipticity of the Cauchy-Riemann operator. It is well known (see for instance [10, 5]) that R^{-1} is a bounded operator of order -1 in the Sobolev space $H^m \times H^m$; i.e., we have $R^{-1} : H^m \times H^m \rightarrow H^{m+1} \times H^{m+1}$ as a bounded bijective operator.

2.3 Approximating the CEC based Model

In this section we show that for a specific choice of the additional constraint our model closely approximates the CEC based model. To establish this we first consider the two constrained optimization problem and their associated augmented Lagrangian framework. Consider the CEC based model:

$$\min_{\mathbf{v}} J_C(\mathbf{v}) = \int_{\Omega} (f_t + \nabla \cdot (f\mathbf{v}))^2 + \alpha \int_{\Omega} (\|\nabla \bar{u}\|^2 + \|\nabla \bar{v}\|^2), \quad (23)$$

subject to the constraint

$$B\mathbf{v} := \nabla f \cdot \mathbf{v} = -f_t =: c. \quad (24)$$

where $\mathbf{v} = (\bar{u}, \bar{v})$ and α is the regularization parameter. For simplicity in computation throughout this section we fix $\beta = 1$, $\phi(f) = f^2$, $\psi = (\nabla \cdot \mathbf{u})^2$. Let us denote the function spaces $V = H^1(\Omega) \times H^1(\Omega)$ and $H = L^2(\Omega)$. For the purpose of analysis we replace the bounded constraint with an equality constraint. We now consider the augmented Lagrangian $\mathcal{L}_{\tilde{\mu}} : V \times H \rightarrow \mathbb{R}$, $\mu > 0$ for the problem (23)-(24) defined as:

$$\mathcal{L}_{\tilde{\mu}}(\mathbf{v}, \lambda_1) = J_1(\mathbf{v}) + \frac{\tilde{\mu}}{2} \|B\mathbf{v} - c\|^2 + \langle \lambda_1, B\mathbf{v} - c \rangle. \quad (25)$$

The associated constrained optimization problem of our model is

$$J_R(\mathbf{v}) = \int_{\Omega} f^2 (\nabla \cdot \mathbf{v})^2 + \alpha \int_{\Omega} (\|\nabla \bar{u}\|^2 + \|\nabla \bar{v}\|^2), \quad (26)$$

subject to the constraint

$$B\mathbf{v} = c. \quad (27)$$

The associated Augmented Lagrangian then becomes

$$\mathcal{L}_{\mu}(\mathbf{v}, \lambda_1) = J(\mathbf{v}) + \frac{\mu}{2} \|B\mathbf{v} - c\|^2 + \langle \lambda_1, B\mathbf{v} - c \rangle. \quad (28)$$

The relation between the functional J_{HS} , J_R and the continuity model formulation

$$J_C(\mathbf{u}) = \int_{\Omega} (f_t + \nabla \cdot (f\mathbf{u}))^2 + \alpha \int_{\Omega} \{|\nabla u|^2 + |\nabla v|^2\}, \quad (29)$$

can be easily seen to satisfy

$$J_C(\mathbf{u}) = J_{HS}(\mathbf{u}) + J_R(\mathbf{u}) + K(\mathbf{u}),$$

where

$$K(\mathbf{u}) = 2 \int_{\Omega} (f_t + \nabla f \cdot \mathbf{u})(f \nabla \cdot \mathbf{u}).$$

By the Cauchy-Schwarz inequality we have $|K(\mathbf{u})|^2 \leq 2\|f_t + \nabla f \cdot \mathbf{u}\|_2^2 \|f \nabla \cdot \mathbf{u}\|_2^2$. Thus,

$$J_C(\mathbf{u}) = J_R(\mathbf{u}) + O(\sqrt{\epsilon}) \quad \text{whenever} \quad \|f_t + \nabla f \cdot \mathbf{u}\|_2 = O(\epsilon). \quad (30)$$

Heuristically arguing, we can take motivation from (30) and adopt a two phase strategy where we first determine the minimizer of J_{HS} and use this minimizer as an initial condition in the evolutionary PDE associated with (5). Although our model is not derived by a rigorous fluid mechanics, we still demonstrate that our results closely approximate the physics based models for this particular choice of ϕ and ψ . For the remaining discussions in this section we closely follow the results in [13, Chapter 3].

Definition. A point (\mathbf{u}, λ) is said to be a saddle point of (25) if

$$\mathcal{L}_{\tilde{\mu}}(\mathbf{u}, \lambda_1) \leq \mathcal{L}_{\tilde{\mu}}(\mathbf{u}, \lambda) \leq \mathcal{L}_{\tilde{\mu}}(\mathbf{v}, \lambda) \quad \forall (\mathbf{v}, \lambda_1) \in V \times H. \quad (31)$$

Lemma 4. (\mathbf{u}, λ) is a saddle point of (25) iff \mathbf{u} solves the variational problem (23)-(24).

Proof. Let \mathbf{u} solve the variational problem (23)-(24). Then

$$\mathcal{L}_{\tilde{\mu}}(\mathbf{u}, \lambda_1) = \mathcal{L}_{\tilde{\mu}}(\mathbf{u}, \lambda).$$

since $B\mathbf{u} = c$. Also $J_R(\mathbf{u}) \leq J_R(\mathbf{v})$ for all \mathbf{v} since \mathbf{u} solves (23). This leads to the second inequality

$$\mathcal{L}_{\tilde{\mu}}(\mathbf{u}, \lambda) \leq \mathcal{L}_{\tilde{\mu}}(\mathbf{v}, \lambda).$$

Conversely assume that (31) holds. Then by the first inequality we have

$$\langle \lambda_1, B\mathbf{u} - c \rangle \leq \langle \lambda, B\mathbf{u} - c \rangle \quad \text{implies} \quad \langle \lambda_1 - \lambda, B\mathbf{u} - c \rangle \leq 0,$$

from which we conclude $B\mathbf{u} = c$. From the second inequality we have

$$J_C(\mathbf{u}) + \frac{\tilde{\mu}}{2} \|B\mathbf{u} - c\|^2 + \langle \lambda, B\mathbf{u} - c \rangle \leq J_C(\mathbf{v}) + \frac{\tilde{\mu}}{2} \|B\mathbf{v} - c\|^2 + \langle \lambda, B\mathbf{v} - c \rangle,$$

for all $\mathbf{v} \in V$. We make a change of variable $\mathbf{v} = \mathbf{u} + t(\mathbf{w} - \mathbf{u})$ for all $\mathbf{w} \in V$ and $0 \leq t \leq 1$. Now

$$\begin{aligned} \langle \lambda, B\mathbf{v} - c \rangle - \langle \lambda, B\mathbf{u} - c \rangle &= \langle \lambda, B(\mathbf{u} + t(\mathbf{w} - \mathbf{u})) - c \rangle - \langle \lambda, B\mathbf{u} - c \rangle \\ &= \langle \lambda, B(\mathbf{u} + t(\mathbf{w} - \mathbf{u})) - c - B\mathbf{u} + c \rangle \\ &= t \langle \lambda, B(\mathbf{w} - \mathbf{u}) \rangle. \end{aligned} \quad (32)$$

Similarly

$$\begin{aligned} \frac{\tilde{\mu}}{2} \|B\mathbf{v} - c\|^2 - \frac{\tilde{\mu}}{2} \|B\mathbf{u} - c\|^2 &= \frac{\tilde{\mu}}{2} \|B(\mathbf{u} + t(\mathbf{w} - \mathbf{u})) - c\|^2 - \frac{\tilde{\mu}}{2} \|B\mathbf{u} - c\|^2 \\ &= \frac{\tilde{\mu}t^2}{2} \|B(\mathbf{w} - \mathbf{u})\|^2. \end{aligned} \quad (33)$$

Finally combining the terms we obtain

$$J_C(\mathbf{u} + t(\mathbf{w} - \mathbf{u})) - J_C(\mathbf{u}) + t \langle \lambda, B(\mathbf{w} - \mathbf{u}) \rangle + \frac{\tilde{\mu}t^2}{2} \|B(\mathbf{w} - \mathbf{u})\|^2 \geq 0.$$

By convexity of J_C we get

$$t(J_C(\mathbf{w}) - J_C(\mathbf{u})) + t\langle \lambda, B(\mathbf{w} - \mathbf{u}) \rangle + \frac{\tilde{\mu}t^2}{2}\|B(\mathbf{w} - \mathbf{u})\|^2 \geq 0.$$

Dividing throughout by t and taking limit as $t \rightarrow 0$ we obtain

$$J_C(\mathbf{w}) - J_C(\mathbf{u}) + \langle \lambda, B(\mathbf{w} - \mathbf{u}) \rangle \geq 0 \quad \forall \mathbf{w} \in V \text{ and } \lambda \in H. \quad (34)$$

Consequently \mathbf{u} solves the variational problem (23). \square

Lemma 5. The tuple (\mathbf{u}, λ) is also the saddle point of the unconstrained optimization problem (28).

Observe that the augmented Lagrangian (25) can be reformulated as

$$\mathcal{L}_{\tilde{\mu}}(\mathbf{v}, \lambda_1) = J(\mathbf{v}) + \frac{\tilde{\mu}}{2}\|B\mathbf{v} - c\|^2 + \langle \lambda_1 + 2f\nabla \cdot \mathbf{v}, B\mathbf{v} - c \rangle. \quad (35)$$

The parameter $\tilde{\mu}$ can be chosen as large as necessary. The unknown λ_1 is obtained by the Uzawa iteration

$$\lambda_1^{(n+1)} = \lambda_1^{(n)} + 2fd^{(n)} + \rho^{(n)}(B\mathbf{v}^{(n)} - c), \quad (36)$$

where $d^{(n)} = \nabla \cdot \mathbf{v}^{(n)}$. In general it is not known whether the term $fd^{(n)}$ remains bounded or blow up. But because of the implicit diffusion phenomena governing the divergence of the flow we can rely upon the semigroup techniques to validate that this term actually remains bounded. In the subsequent section we will demonstrate the effect of diffusion on both the constraints. In fact by the causality property derived by the semigroup theory it is evident that the decoupled system essentially retains the spatial structure of the divergence and vorticities emerging out of the initialization.

The starting point is the crude pixel correspondence obtained from the Horn and Schunck optical flow $\mathbf{v}^{(0)}$ obtained within a tolerance limit δ_{HS} prescribed by Liu-Shen [19]. Observe that when the optical flow constraint is exactly satisfied then the formulations (23) and (26) coincide. However in reality due to numerical errors and approximations, the constraints are never exactly met. The algorithm above can be viewed in two phases where: in the first phase, it is purely diffusion while in the second phase it is the bounded constraint which in turn approximates the continuity equation constraint. This happens mainly because a part of the OFC is already embedded in the CEC.

This relaxation is allowed so that we do not move too far away from the constraint and to ensure that the tolerance $\epsilon_1^{(n)}$ doesn't become too small. The updates $\mathbf{v}^{(n)}$ happen by solving the Euler-Lagrange equations iteratively using standard finite difference techniques. $d^{(n)}$ is updated by the relation

$$d^{(n)} = S(t)d^{(n-1)},$$

where the map $S(t) : u_0 \mapsto u(t) := G_k(\cdot, t) * u_0$ form a linear, continuous semigroup of contractions in $L^2(\Omega)$. The key steps in the algorithm are actually (10-13). We reach here when the additional term is not within the convergence tolerance. We update the multiplier $\lambda_1^{(n)}$ of the Uzawa iteration. To show that the multipliers $\lambda_1^{(n)}$ converges we use the semigroup techniques. We proceed as follows. Consider the i^{th} equation of (36):

$$\lambda_1^{(i+1)} - \lambda_1^{(i)} = 2fd^{(i)} + \rho^{(i)}(B\mathbf{v}^{(i)} - c), \quad 1 \leq i \leq n.$$

Algorithm 1 Bounded Constraint Algorithm

```

1: procedure BCA
2:   Set  $\lambda^{(0)}, \rho^{(0)}$ . Choose  $\epsilon_1^{(0)}, \epsilon_2^{(0)}$ .
3:   Obtain initial HS optical flow  $\mathbf{v}^{(0)}$ 
4:   for  $n = 1, 2, \dots$  until convergence do
5:     update  $\mathbf{v}^{(n)}, d^{(n)}$ 
6:     if  $\|B\mathbf{v}^{(n)} - c\| \leq \max\{\epsilon_1^{(n)}, 2\delta_{\text{HS}}\}$ 
7:       if  $\|fd^{(n)}\| \leq \epsilon_2^{(n)}$ 
8:         break;
9:       else
10:        update  $\lambda^{(n)}$  by (36)
11:         $\rho^{(n+1)} \leftarrow \rho^{(n)}$ 
12:         $\epsilon_1^{(n+1)} \leftarrow \epsilon_1^{(n)} / \rho^{(n+1)0.9}$ 
13:         $\epsilon_2^{(n+1)} \leftarrow \epsilon_2^{(n)} / \rho^{(n+1)}$ 
14:      else
15:        update  $B\mathbf{v}^{(n)} - c$ 
16:         $\lambda^{(n+1)} \leftarrow \lambda^{(n)}$ 
17:         $\rho^{(n+1)} \leftarrow 100\rho^{(n)}$ 
18:         $\epsilon_1^{(n+1)} \leftarrow \epsilon_1^{(n)} / \rho^{(n+1)0.1}$ 
19:         $\epsilon_2^{(n+1)} \leftarrow \epsilon_2^{(n)} / \rho^{(n+1)}$ 

```

Adding the n equations we obtain

$$\begin{aligned} \lambda_1^{(n+1)} - \lambda_1^{(0)} &= 2f[d^{(n)} + \dots + d^{(0)}] + \rho^{(n)}(B\mathbf{v}^{(n)} - c) + \dots + \rho^{(0)}(B\mathbf{v}^{(0)} - c) \\ &= 2f[S(t)^n d^{(0)} + \dots + d^{(0)}] + \rho^{(n)}(B\mathbf{v}^{(n)} - c) + \dots + \rho^{(0)}(B\mathbf{v}^{(0)} - c). \end{aligned}$$

Therefore

$$\lambda_1^{(n+1)} - \lambda_1^{(0)} = 2f\left[\sum_{i=0}^n S(t)^i\right]d^{(0)} + \sum_{i=0}^n \rho^{(i)}(B\mathbf{v}^{(i)} - c).$$

Hence

$$\|\lambda_1^{(n+1)} - \lambda_1^{(0)}\|_{L^2} \leq 2\|f\|\left\|\left[\sum_{i=0}^n S(t)^i\right]d^{(0)}\right\| + \sum_{i=0}^n |\rho^{(i)}| \|B\mathbf{v}^{(i)} - c\|. \quad (37)$$

Let us first consider the second sum in (37). Following the algorithm we note that $\|B\mathbf{v}^{(n)} - c\| \leq C\epsilon_1^{(n)}$. Since the tolerance limit $\epsilon_1^{(n)}$ is tightened after every update, there exists a N such that for $n > N$ we can choose a $M > 0$ such that $\epsilon_1^{(n)} \leq M/(n+1)^2$ as long as $\epsilon_1^{(n)} > 2\delta_{\text{HS}}$. Thus

$$\|B\mathbf{v}^{(n)} - c\| \leq C \frac{M}{(n+1)^2}.$$

Also as step (11) of the algorithm suggests the tuning parameter $\rho^{(n+1)}$ is assigned the value of the previous iteration $\rho^{(n)}$. Thus this value is fixed as long as the steps (10)-(13) run. Let us denote this fixed value by m . Combining these discussions we obtain

$$\sum_{i=0}^n |\rho^{(i)}| \|B\mathbf{v}^{(i)} - c\| \leq mCM \sum_{i=0}^n \frac{1}{(i+1)^2},$$

which remains finite as n becomes large. Suppose it takes n iterations where $\epsilon_1^{(n)} > 2\delta_{\text{HS}}$. From the $(n+1)^{\text{th}}$ iteration when $\epsilon_1^{(n+j)} < 2\delta_{\text{HS}}, j = 1, 2, \dots$ the upper bound becomes $2\delta_{\text{HS}}$. Combining we have

$$\sum_{i=0}^n |\rho^{(i)}| \|B\mathbf{v}^{(i)} - c\| \leq r,$$

where

$$r = \max \left\{ \frac{\pi^2}{6} mCM, 2\delta_{\text{HS}} \right\}.$$

which remains finite as $n \rightarrow \infty$. Since $S(t)$ is a contraction we observe that as $n \rightarrow \infty$ the series of operators in the first term of (37) converges to $(I - S(t))^{-1}$ which is a bounded operator. This shows the convergence of the multipliers $\lambda_1^{(n)}$.

2.3.1 Details of the Bounded Constraint Algorithm (1)

Since the functionals in our work make it convenient for an efficient implementation of the augmented Lagrangian scheme we have lesser new variables. Based on the augmented Lagrangian scheme, the Bounded Constraint Algorithm (1) has outer and inner iterations. At the outer iterations, we formulate the modified augmented Lagrangian function and initialize the subproblem. The rest of the steps in the outer iterations check for convergence and update the penalty parameter. The inner iterations solve the subproblem and update the lagrange multiplier.

At the initialization step, we use Horn and Schunck (HS) optical flow estimator with an L^2 regularizer to obtain $\mathbf{v}^{(0)}$. For the continuity equation case, with this initialization, the results of the algorithm can be fine-tuned corresponding to the penalty parameter μ with the key observation that the HS optical flow is also a divergence-free approximation for the continuity equation based fluid flow. This observation was also used by Liu-Shen to improve the rate of convergence in their implementation.

At step 5 of the outer iterations we discretize and solve the Euler-Lagrange equations of (5) for particular ϕ and ψ . For instance, for our main case corresponding to the continuity based model $\phi = f^2$ and $\psi = (\nabla \cdot \mathbf{v})^2$, the scheme is

$$\mathbf{P}\mathbf{v}^{(n+1)} = \mathbf{b}\mathbf{v}^{(n)}, \quad (38)$$

where

$$\mathbf{P} := \begin{bmatrix} \alpha + \frac{2\beta f^2}{\Delta x^2} & 0 \\ 0 & \alpha + \frac{2\beta f^2}{\Delta y^2} \end{bmatrix}, \quad \mathbf{b}\mathbf{v}^{(n)} = \begin{bmatrix} \alpha(M * u^{(n)}) + \beta \frac{\partial}{\partial x}[f^2 d^{(n)}] \\ \alpha(M * v^{(n)}) + \beta \frac{\partial}{\partial y}[f^2 d^{(n)}] \end{bmatrix}, \quad (39)$$

and M is the nine point approximation stencil of the laplacian. As mentioned above

$$d^{(n)} = G_k(\cdot, t) * d^{(n-1)},$$

where G_k is the diffusion kernel associated with the operator $k\Delta$. This semigroup structure allows the process to preserve the spatial characteristics of the divergence and the vorticities.

We subsequently check for the convergence criteria as mentioned in steps 6 and 7. If both the criteria are satisfied then the required approximation is met and the algorithm

terminates. If step 7 is not satisfied then we enter the inner iterations and run through steps 10 to 13 where we update the Lagrange multiplier λ while the penalty parameter μ is not modified. For a sufficiently large μ we choose λ as a function in $L^2(\Omega)$. The convergence of $\lambda^{(n)}$, which is discussed in the previous section, is critical for the well-posedness of the augmented Lagrangian approach.

The outer iteration steps 15 to 19 are executed when the convergence criteria in step 6 fail. In this case, first, the optical flow constraint is updated. Then, to preserve the convergence and to ensure no occurrence spurious updates the Lagrange multiplier is assigned the value from the previous iteration. However, in our case as the bounded constraint being a divergence-free approximation of the continuity model and by the continuity of the semigroup operators on the Sobolev space, the penalty parameter will be reasonably small. It is also important to note the order to which the tolerance $\epsilon_1^{(n)}$ is tightened in both the inner and outer iterations. Unlike the outer iterations, the inner iterations ensure the tolerance doesn't fall too rapidly by considering a power 0.9.

3 Results

In this section, we show the running of Algorithm (1) on some example sets and compare our results with the Liu-Shen continuity based model. Since our algorithm is not based on coarse-to-fine implementation we only consider the single (finer) level implementation of Liu-Shen. Moreover, coarse-to-fine implementation has a bigger spatial neighbourhood and thus makes the flow isotropic.

We first consider the Oseen vortex pair and consider the case $\phi(f) = f^2$ and $\psi = (\nabla \cdot \mathbf{u})^2$ which approximates the continuity based model. The Oseen vortex pair is a synthetic PIV sequence of dimension 500×500 . The vortices are placed centered at the positions (166.7, 250) and (333.3, 250). The circumferential velocity is given by $v_\theta = (\Gamma/2\pi r)[1 - \exp(-r^2/r_0^2)]$ with the vortex strength $\Gamma = \pm 7000$ pixels²/s and vortex core radius $r_0 = 15$ pixels. For more details see [18].

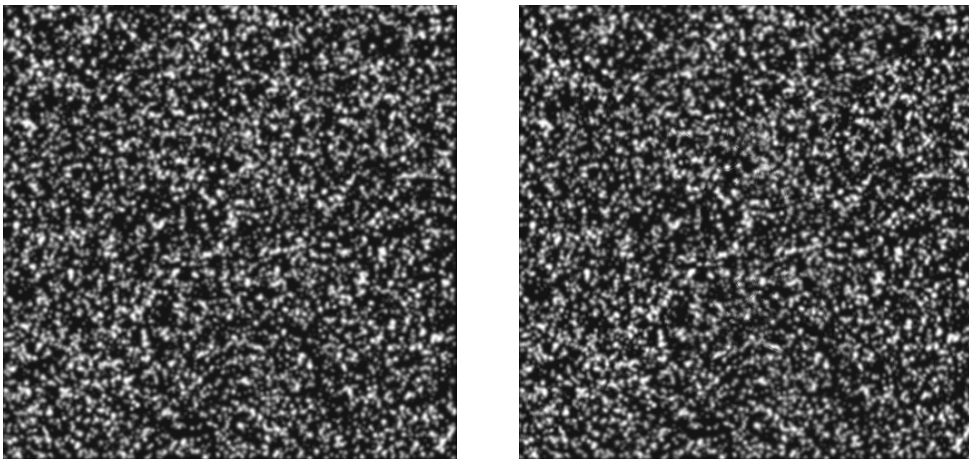


Figure 1: Oseen vortex pairs

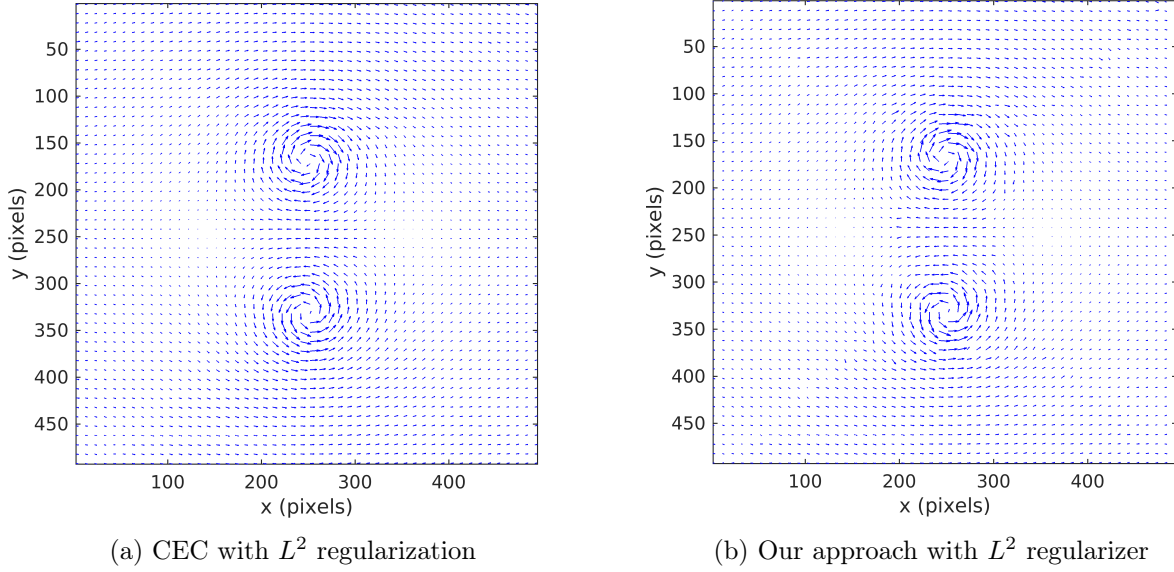


Figure 2: Vorticity field of the Oseen vortex pairs

Figure (2) shows that the vorticity field obtained through our constraint-based refinement algorithm is very close to the Liu-Shen continuity equation based model (CEC). In the Liu-Shen implementation of CEC based model, the Lagrange multiplier in the HS-estimator is chosen to be 20 and in the Liu-Shen estimator, it is fixed at 2000. They observed that for a refined velocity field it does not significantly affect the velocity profile in a range of 1000–20,000 except the peak velocity near the vortex cores in this flow. The weight parameters α and β in our algorithm are chosen to be 100 and 0.01 respectively. It was observed experimentally that the numerical scheme converges when the ratio β/α is less than or equal to 10^{-4} .

In our experiment we have initialized $\lambda^{(0)} = 0$. We studied the convergence rate of the L^2 norms of $fd^{(n)}$ and $B\mathbf{v}^{(n)} - c$ with respect to the number of iterations. We observed the L^2 norm values of $fd^{(n)}$ falls rapidly from 1800 to 600 within 150 iterations after which the decay slowed down. This rapid decay can be explained by the ‘anisotropic’ Gaussian convolution (Equation 22) in the semigroup operator. Similarly the L^2 norm values of $B\mathbf{v}^{(n)}$ fell from 214 to 196 over 200 iterations. This slow decay is because the optical flow constraint does not involve any derivatives of the unknowns u and v as a result of which the diffusion is slower. The tuning parameter ρ was fixed at 0.5. Thus for the Oseen vortex pair the value $\|\lambda^{(n+1)}\|_{L^2}$ falls from 1907 to 698 over 150 iterations and then continues to decay at a slower rate. This numerical experimentation shows the convergence of λ .

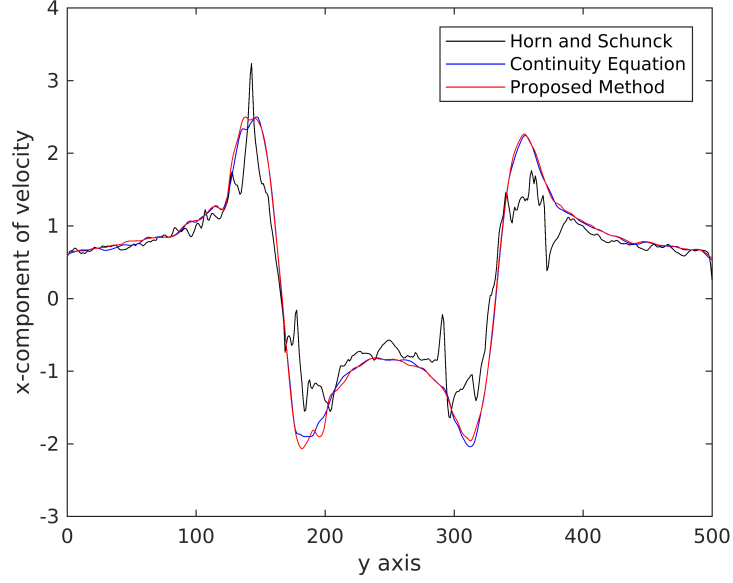


Figure 3: Distribution of the x -component of the velocity extracted from the grid images for the oseen vortex pair

Performing a similar analysis as in [24] we plot the distribution of the x -component of the velocity to obtain Figure (3). This plot compares the distribution of the x -component of the velocity extracted from the grid images for the HS model, CEC model and our constraint-based refinement model. The profiling clearly shows the closeness of our algorithm to the continuity equation based model. From the figure, it is also seen how the Horn and Schunck model underestimates the flow components, especially near the vortex cores.

We now show the results for the cloud sequence. In this sequence, the movement of the fluid exhibits both formation of a vortex as well as a movement of fluid parcels. The distribution of the strength of the vortices in the cloud sequence obeys a Gaussian distribution of mean 0 and standard deviation of $3000 \text{ (pixels)}^2/\text{s}$.

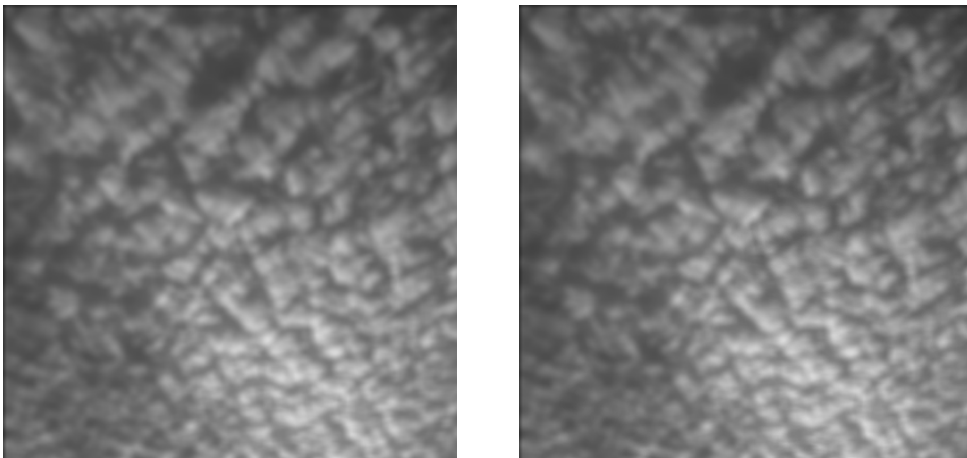


Figure 4: Cloud sequence

The comparison of the vorticity plots are shown below:

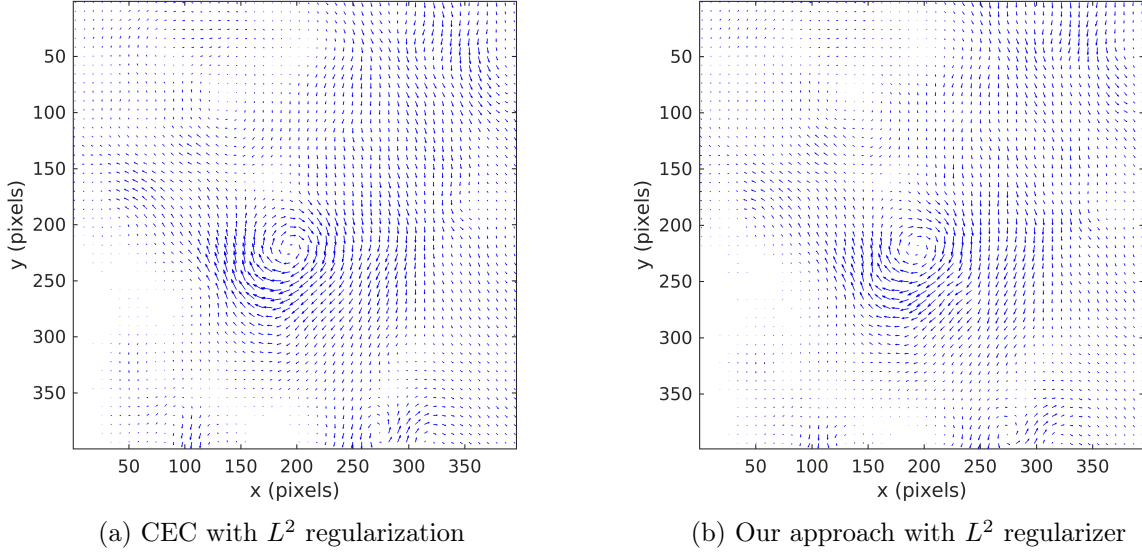


Figure 5: Vorticity field of the Cloud sequence

As seen from Figure (5) the isotropic behaviour of the regularization is seen more on the continuity equation based implementation because of the denseness of the flow. Also by increasing the number of iterations we have observed that the effect of diffusion makes the vortices completely circular. The distribution of the x -component of the velocity for the cloud sequence is shown below. The Horn and Schunck estimator tends to over estimate at the peaks.

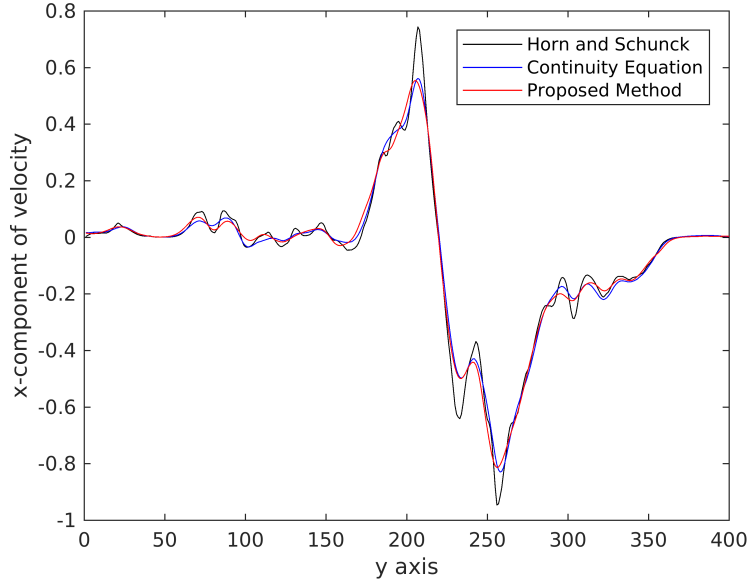


Figure 6: Comparison between the distributions of the x -component of the velocity extracted from the grid images for the cloud sequence

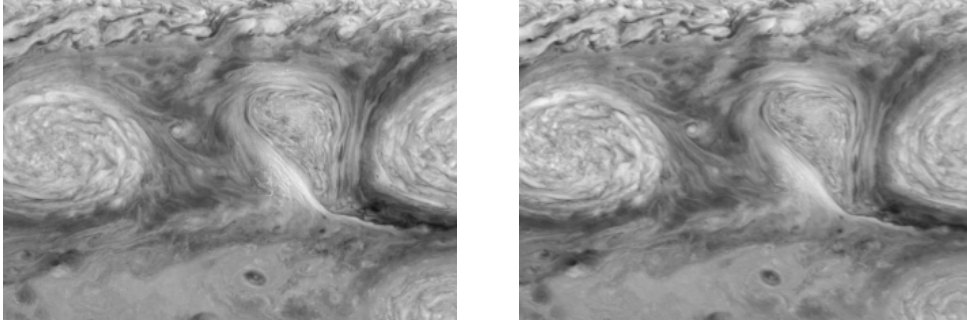


Figure 7: Jupiter's white oval sequence

Figure (7) shows Jupiter's white oval sequence. They are distinct storms on Jupiter's atmosphere captured by NASA's Galileo spacecraft at a time-lapse of one hour, see [18]. Due to its diversity, this is an interesting sequence for the application of optical flow methods. Firstly, the motion patterns are continuous in this sequence. Secondly, it was observed that the sun's illumination influenced the subsequent frame considerably in a non-uniform way. To compensate the illumination effects one needs to adjust the illumination variation before applying the optical flow method. In the Liu-Shen implementation, an illumination correction is employed by normalizing the intensities and performing a local intensity correction using Gaussian filters. Figure (8) shows the results of their implementation of the CEC model.

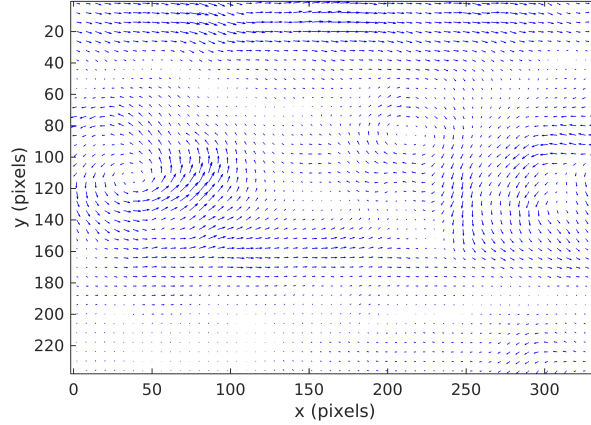
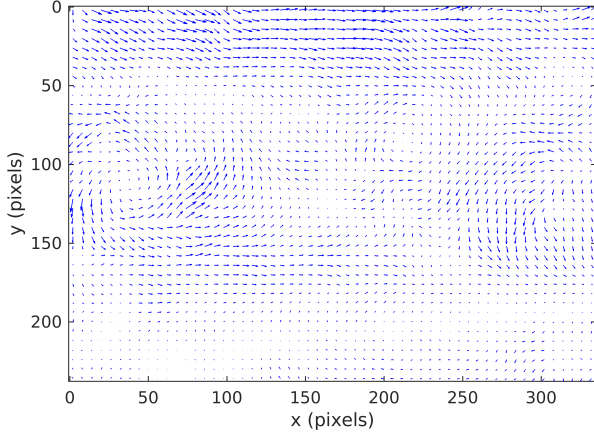
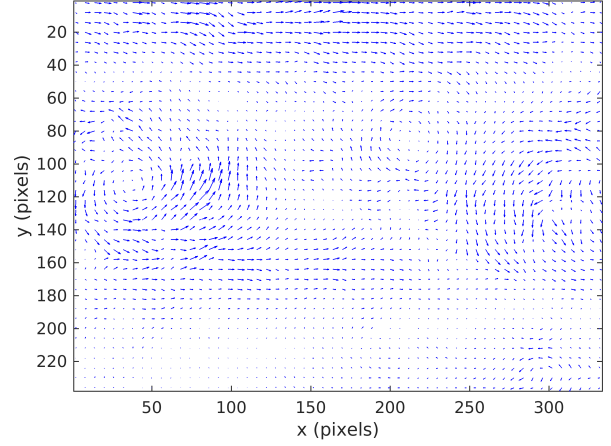


Figure 8: CEC with illumination correction and L^2 regularization for Jupiter's white oval sequence



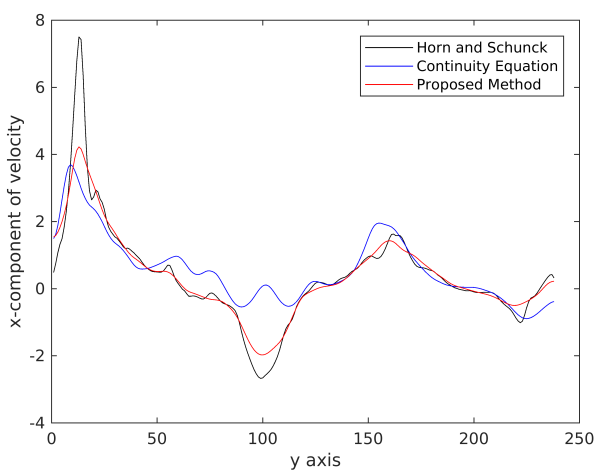
(a) Our approach without illumination correction



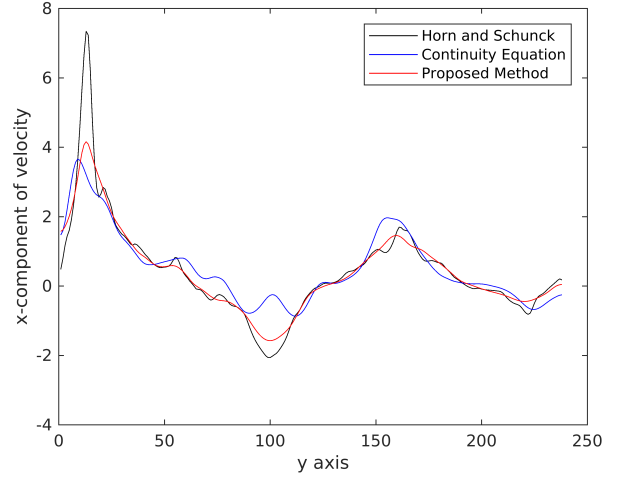
(b) Our approach with illumination correction

Figure 9: Vorticity plot of the Jupiter's white oval sequence

The flow patterns are not very well captured in our constraint based refinement flow as seen in the first plot of Figure (9). This is because we have not taken into account the illumination correction for the dataset. The second plot in Figure (9) shows the refinement algorithm with illumination correction. As seen from the two vorticity fields the plot on which illumination correction has been applied captures the vortices better. This can be further illustrated with the distribution of the x -component of the velocity as shown below:



(a) Our refinement without illumination correction



(b) Our with illumination correction

Figure 10: Effect of the illumination correction on the distribution of the x -component of the velocity for Jupiter's white oval sequence

As seen from Figure (10) there is a large deviation near the vortex region when illumination correction is not taken into account. The deviation is minimized to a great extent as can be seen from the second image. The reason for our results (even with illumination

correction) not being close to the illumination corrected CEC is because of the direct dependency of the process on the image data.

Rather than correcting the illumination by modifying the scheme we choose a flow-driven refinement process (independent of image data) and perform a diffusion on the curl component. In order to achieve this, we consider the case $\phi(f) = 1$ and $\psi = (\nabla_H \cdot \mathbf{u})^2$ where ∇_H is the Hamiltonian gradient also referred to as the symplectic gradient in literature [20]. Introducing the symplectic gradient switches the roles of divergence and curl in the Equation (10) and the analysis follows in the same lines.

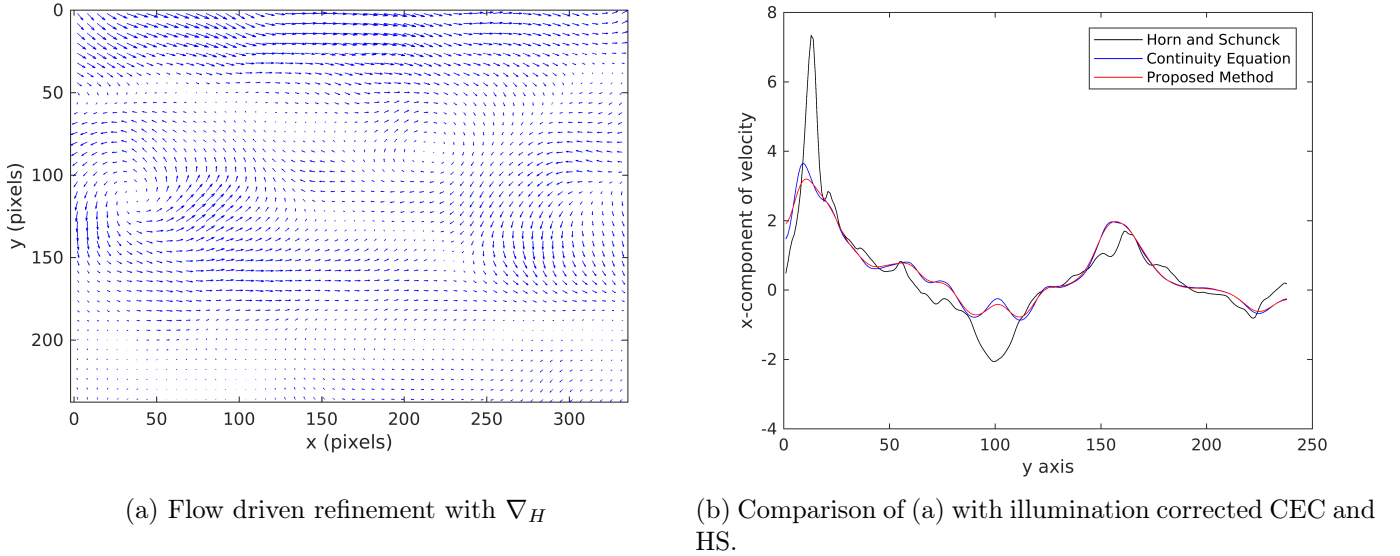


Figure 11: Plots of the Jupiter's white oval sequence with $\phi(f) = 1, \psi(\mathbf{u}) = (\nabla_H \cdot (\mathbf{u}))^2$ and without illumination correction.

Figure (11)(a) gives the vorticity plot obtained by our constraint-based refinement process $\phi(f) = 1$ and $\psi(\mathbf{u}) = (\nabla_H \cdot \mathbf{u})^2$ of Jupiter's white oval sequence. The ovals are clearly seen in the figure. Figure (11)(b) gives the distribution of the x -component of the velocity given in Figure (11)(a) and illumination corrected CEC and illumination corrected HS flow estimators. It should be noted that the flow plots of our refinement process without illumination correction is close to the CEC with illumination correction.

Conclusion. In this work, we have proposed a general framework for a constraint-based refinement of optical flow using variational methods. We have studied the well-posedness and the regularity of the solutions using evolutionary PDE approach in a Hilbert space setting. We have also shown that our coupled system can be decoupled by the Cauchy-Riemann operator. The decoupled system leads to the diffusion of the curl and the multiplicative perturbation of the laplacian of the divergence of the flow. For a particular choice of additional constraints, we have shown that our model closely approximates the continuity equation based model. Finally, we have shown the results of our algorithm on different datasets. We have also compared and shown the effect of the image data term on the refinement process by considering two different additional constraints. We also believe that our approach to refinement of the optical flow can be extended to a learning paradigm.

Acknowledgements. We express our deep sense of gratitude to and dedicate this paper to Bhagawan Sri Sathya Sai Baba, Revered Founder Chancellor, SSSIHL. We would like to thank Dr. Shailesh Srivastava for his insight into obtaining the velocity plots. The first author acknowledges the Sri Sathya Sai Central Trust for a partial funding of the research.

References

- [1] Alvarez L., Esclarin, J., Lefebure M., Sánchez J.: A PDE model for computing optical flow, Proc. XVI Congreso de Ecuaciones Diferenciales y Aplicaciones, 1349-1356 (1999).
- [2] Altomare P. , Milella S., Musceo G.: Multiplicative Perturbation of the Laplacian and related Approximation Problems, Journal of Evolution Equations, 771-792, (2011).
- [3] Aubert G., Deriche R., Kornprobst P.: Computing Optical Flow via Variational Techniques, SIAM Journal of Applied Mathematics, Vol. 60, 156-182 (1999).
- [4] Aubert G., Kornprobst P.: Mathematical Problems in Image Processing, Calculus of Variations and Partial Differential Equations, Springer, New York (2002).
- [5] Brezis H., Functional Analysis, Sobolev Spaces and Partial Differential Equations, Springer, New York (2011).
- [6] Chen X., Zillé P., Shao L., Corpetti T.: Optical Flow for Incompressible Turbulence Motion Estimation. Experiments in Fluids, Springer Verlag (Germany), (2015).
- [7] Corpetti T., Mémin E., Pérez P.: Estimating Fluid Optical Flow, Proceedings of the 15th International Conference on Pattern Recognition, ICPR-2000, Vol. 3, 1033-1036 (2000).
- [8] Corpetti T., Heitz D., Arroyo G., Mémin E., Santa-Cruz A.: Fluid Experimental Flow Estimation based on an Optical Flow Scheme, Experiments in Fluids, (2006).
- [9] Dacorogna B.: Direct Methods in Calculus of Variations, Springer, New York (2008).
- [10] Darko P.: On L^p Sobolev Space Estimates for the Inhomogeneous Cauchy-Riemann Equation on Polycylinders, Complex Variables, Vol. 38, 367-373 (1999).
- [11] Eidus P.: The Perturbed Laplace Operator in a weighted L^2 space, Journal of Functional Analysis, 100, 400-410 (1991).
- [12] Evans L.C.: Partial Differential Equations, Second Edition, Americal Mathematical Society.
- [13] Glowinski R., Le Tallec P., Augmented Lagrangian and Operator-Splitting Methods in Nonlinear Mechanics, SIAM, Philadelphia (1989).
- [14] Heitz D., Mémin E., Schnörr C.: Variational Fluid Flow measurements from Image Sequences: Synopsis and Perspectives, Experiments in Fluids, 48, 369–393 (2010).
- [15] Le Dret H., Lucquin B.: Partial Differential Equations: Modeling, Analysis and Numerical Approximation, Birkhäuser, Springer (2016).

- [16] Hinterberger W., Scherzer O., Schnörr C., Weickert J.: Analysis of Optical Flow Models in the Framework of Calculus of Variations, *Numer. Funct. Anal. and Optimiz.*, 23(1&2), 69-89 (2002).
- [17] Horn B.K.P., Schunck B.G.: Determining Optical Flow, *Artificial Intelligence*, Vol. 17, 185-203 (1981).
- [18] Liu T.: OpenOpticalFlow: An Open Source Program for Extraction of Velocity Fields from Flow Visualization Images, *Journal of Open Research Software*, 5:29 (2017).
- [19] Liu T., Shen L.: Fluid Flow and Optical Flow, *Journal of Fluid Mechanics*, 614, 253-291 (2008).
- [20] Luttmann A., Bollt E.M., Basnayake R., Kramer S., Tufillaro N.B.: A Framework for Estimating Potential Fluid Flow from Digital Imagery, *Chaos: An Interdisciplinary Journal of Nonlinear Science*, Vol. 23, no-3 (2013).
- [21] Sapiro G.: *Geometric Partial Differential Equations and Image Analysis*, Cambridge University Press, New York (2001).
- [22] Schnörr C.: Determining optical flow for irregular domains by minimizing quadratic functionals of a certain class, *International Journal of Computer Vision*, Vol. 6, 25-38 (1991).
- [23] Vold, E., Yin, L., Taitano, W., Molvig, K., Albright, B., Diffusion-driven fluid dynamics in ideal gases and plasmas, *Physics of Plasmas* 25, 062102, (2018).
- [24] Wang B., Cai Z., Shen L., Liu T.: An Analysis of Physics-based Optical Flow, *Journal of Computational and Applied Mathematics*, 276, 62-80 (2015).
- [25] Weickert J., Schnörr C.: A Theoretical Framework for Convex Regularizers in PDE-based Computation of Image Motion, *International Journal of Computer Vision*, 45, 245-264 (2001).
- [26] Wildes R.P., Amabile M.J., Lanzillotto A., Leu T.: Recovering Estimates of Fluid Flow from Image Sequence Data, *Computer Vision and Image Understanding*, 80, 246-266 (2000).